Photofission of ^{197}Au at Intermediate Energies

H. Haba,*[,a] M. Igarashi,[b] K. Washiyama,[a] H. Matsumura,[a] M. Yamashita,[a] K. Sakamoto,†[,a,b] Y. Oura,[c] S. Shibata,[d] M. Furukawa,[e] and I. Fujiwara[f]

[a]*Division of Physical Sciences, Graduate School of Natural Science and Technology, Kanazawa University, Kanazawa-shi, Ishikawa 920-1192, Japan*
[b]*Department of Chemistry, Faculty of Science, Kanazawa University, Kanazawa-shi, Ishikawa 920-1192, Japan*
[c]*Department of Chemistry, Graduate School of Science, Tokyo Metropolitan University, Hachioji-shi, Tokyo 192-0397, Japan*
[d]*Research Reactor Institute, Kyoto University, Sennan-gun, Osaka 590-0494, Japan*
[e]*Faculty of Environmental and Information Sciences, Yokkaichi University, Yokkaichi-shi, Mie 512-8512, Japan*
[f]*Department of Economics, Faculty of Economics, Otemon-Gakuin University, Ibaraki-shi, Osaka 567-8502, Japan*

Received: April 4, 2000; In Final Form: June 30, 2000

The reaction yields of 58 radionuclides with the mass number A = 42–131 produced in the photofission of ^{197}Au by bremsstrahlung of end-point energies (E_0) from 300 to 1100 MeV have been measured using the catcher foil technique. The reaction yields increase steeply with an increase of E_0 up to 600 MeV and increase gradually above 600 MeV, indicating the resonance-type excitation function attributed to the (3,3) resonance. The charge distribution was found to be well reproduced by a Gaussian function with the most probable charge (Z_p) expressed by a linear function of A, i.e., $Z_p = RA + S$, and with the A-independent full width at half maximum ($FWHM_{CD}$). The charge distribution parameters R, S, and $FWHM_{CD}$ were found to be independent of E_0 above 600 MeV, reflecting the resonance nature in photonuclear reactions at intermediate energies. The weighted mean values at $E_0 \geq 600$ MeV were $R = 0.424 \pm 0.001$, $S = 0.7 \pm 0.1$, and $FWHM_{CD} = 2.2 \pm 0.1$ charge unit (c.u.). Based on these parameters, the symmetric mass yield distributions with the most probable mass A_p of 92 ± 1 mass unit (m.u.) and the width $FWHM_{MD}$ of 39 ± 1 m.u. were obtained. The characteristics of the charge and mass yield distributions were discussed by referring to the literature data including those of proton-induced reactions.

1. Introduction

Photofission processes at intermediate energies are expected to be unique for investigating the complex dynamics of excitation in heavy nuclei when compared with hadron-induced fission, because photons interact electromagnetically with nuclei through giant dipole resonance, quasi-deuteron mechanism, and (3,3) resonance. For preactinide nuclei, the photofission processes opened by the quasi-deuteron mechanism and the (3,3) resonance absorption are especially important due to their high fission thresholds of > 20 MeV that suppress the fission channels opened by the giant dipole resonance. Thus a photon of an energy above 20 MeV sees all nucleons inside a nucleus identically and interacts with a nucleon-nucleon pair or a single nucleon, transferring its kinetic energy effectively but comparatively little angular momentum to the nucleus. In this context photofission is quite different from hadron-induced fission. A hadron, which possesses large angular momentum, collides with a single nucleon in the surface region of the nucleus through the strong nucleon-nucleon interaction. It is of interest to investigate whether there exist similarities or not in the final steps in these two types of nuclear reactions.

Previously, we[1–3] measured the photospallation yields for ^{nat}V, ^{59}Co, ^{nat}Cu, ^{89}Y, ^{127}I, ^{133}Cs, ^{nat}La, and ^{197}Au targets at the bremsstrahlung end-point energies (E_0) of 30–1050 MeV, and analyzed them by the five-parameter charge distribution and mass yield distribution (CDMD) formula given by Rudstam.[4] From the slope of the mass-yield curve (P) and the total inelastic cross section ($\hat{\sigma}$) in the formula, some anomalous behaviors of the energy-absorption and energy-dissipation mechanisms were suggested for heavy targets with the target mass number $A_t \geq 150$. Recently a systematic yield measurement of the (γ, $\pi^- x$n) reactions for x = 0–9 on targets ranging from ^{7}Li to ^{209}Bi were also reported by our group.[5] It was found that changes in the yield profiles for targets heavier than A_t = 100 might be associated with pronounced nuclear medium effects giving rise to more excessive excitation as compared with medium-heavy targets with $A_t < 100$. These findings have motivated us to an investigation on the fission process, which is characteristic of heavy nuclei and competes with spallation, fragmentation, and also simple photopion reactions.

The photofission study of ^{197}Au is appropriate for this purpose, because the yields of the competing spallation, fragmentation, and simple photopion reactions have already been obtained by our group.[2,3,5,6] The total photofission yields and/or cross sections on ^{197}Au have been extensively measured with ionization chambers, and solid-state track detectors so far.[7–21] A few works[22,23] measuring charge distribution and/or mass distribution, which are further essential for fission mechanisms, were performed in the past. Komar et al.[22] reported the symmetric mass yield distribution with the full width at half maximum $FWHM_{MD}$ = 40 m.u. by the coincident energy measurements of fission fragment pairs at E_0 = 1000 MeV, assuming the mass number of the fissioning nucleus to be A_f = 194. On the other hand, Areskoug et al.[23] measured the relative yields of 29 radionuclides produced from ^{197}Au at E_0 = 600 MeV using the catcher foil technique. They analyzed the yields of 22 fission products by a six-parameter charge distribution and mass yield distribution formula, and reported a Gaussian mass distribution with the most probable mass A_p = 92.6 ± 0.6 m.u. and $FWHM_{MD}$ = 30.9 ± 1.7 m.u. They concluded that the larger width reported by Komar et al.[22] at E_0 = 1000

*Present address: Japan Atomic Energy Research Institute, Tokai-mura, Naka-gun, Ibaraki 319-1195, Japan. E-mail: haba@popsvr.tokai.jaeri.go.jp.
†Corresponding author. E-mail: kohsakamoto@par.odn.ne.jp. FAX: +81-76-224-8253.

© 2000 The Japan Society of Nuclear and Radiochemical Sciences
Published on Web 12/28/2000

MeV was attributed to the higher photon energy investigated.

In the present work the photofission of ^{197}Au was investigated systematically in the wide E_0 range of E_0 = 300–1100 MeV using the thick-target thick-catcher method with the aid of intensive chemical separations. Reported in this paper are the absolute reaction yields of the 58 fission products in the mass range of $42 \le A \le 131$. The charge and mass yield distributions, and total fission yields were deduced and compared with the literature data including those of proton-induced reactions. In a separate paper,[24] the recoil properties of the 29 product nuclei in the mass range of $24 \le A \le 131$ are reported and discussed together with the previous photospallation results and also the literature data on the proton-induced reactions.

2. Experimental

Irradiations by electron-free bremsstrahlung beams with E_0 = 300–1100 MeV in steps of 100 MeV or less were carried out using the 1.3 GeV electron synchrotron of the High Energy Accelerator Research Organization (KEK) at Tanashi. The target consisted of a stack of 40–50 sets of a Au foil (99.99%) of 90 mg/cm^2 in thickness and 2.5 × 2.5 cm^2 in size sandwiched by one pair of Mylar foil of 7.0 mg/cm^2 in thickness and 2.5 × 2.5 cm^2 in size, which collected the recoil nuclei in the forward or backward directions with respect to the beam axis. The stack was vacuum-encapsulated in a polyethylene bag together with additional 40–50 Mylar foils (280–350 mg/cm^2) on the downstream side of the beam, which served as an activation blank. Details of the irradiation were almost the same as described in the previous papers.[1,25,26] The photon intensities evaluated from the monitor reaction of ^{27}Al (γ, 2pn) ^{24}Na (Refs. 27, 28) were 10^9–10^{10} equivalent quanta per second (eq.q./s). A typical irradiation period was 5 h.

After irradiation, about 10 selected Au foils and all of the forward and backward catcher foils from one target pile were collected separately and were assayed for radioactivities nondestructively with high-purity Ge detectors each coupled with a 4 k-channel pulse height analyzer. The other 30–40 Au foils were divided into three portions and subjected to chemical separations of K, Fe, Ni, Zn, Ga, As, Rb, Sr, Y, Zr, Nb, Mo, Ag, and Ba. All of the chemical procedures applied in the present work are described in a separate paper.[29] Radioactivities in the chemically separated samples were also assayed by γ-ray spectrometry. In order to obtain the recoil data of products with low reaction yields, chemical separations of scandium and barium were employed for the Mylar catchers in a separate irradiation at E_0 = 1000 MeV. The identifications of radionuclides were made on the basis of their γ-ray energies and half-lives. The γ-ray intensities were obtained with the automatic peak search program "SPECanal98".[30] The detector efficiency was determined with calibrated ^{152}Eu and ^{182}Ta sources with the same size as the samples. The decay properties of interest such as half-lives, γ-ray energies, and branching ratios [31–33] are summarized in Table 1, together with formation types; I: independent yield, C–: cumulative yield by β^- decay, and C+: cumulative yield by β^+ decay and/or electron capture. This classification was made on the basis of charge distributions of the product nuclei (See sect. 3. 2.), irradiation periods, and times required for chemical separations.

3. Results and Discussion

3.1. Yield Curves. In the present work the radioactivities of 36 product nuclides in the mass range of A = 46–131 were identified both in the forward and backward catcher foils. They are denoted with a label "C" in Table 1. In the nondestructive Au target and/or the chemically separated samples, the radioactivities of 50 nuclides in the mass range of A = 42–131 were identified as denoted with a label "T" in the same table. From the fractions of each nuclide which has recoiled out of the Au target of the thickness W in unit of mg/cm^2 into the forward and backward catcher foils, expressed as $F = N_F/(N_F + N_B + N_{target})$ and $B = N_B/(N_F + N_B + N_{target})$, N being the number of atoms, respectively, the effective mean ranges, FW and BW, in Au were obtained. The mean ranges of ^{46}Sc were calculated by estimating the produced radioactivities in the target on the basis of our yield data at the same E_0.[6] It was found that the effective mean ranges FW and BW are independent of E_0 at the studied E_0.[24] A quantity approximately equal to the mean range of the recoil in the target material, $2W(F+B)$ in unit of mg/cm^2 of Au, was calculated for 28 nuclides in the mass range of A = 46–131, and they are indicated in Figure 1 by open circles as a function of the product mass number A, together with the eight values reported by Areskoug et al.[23] at E_0 = 600 MeV by closed squares. The present results agree well with those by Areskoug et al.[23] within the experimental errors. The $2W(F+B)$ values decrease almost linearly with an increase of A, and no effects attributed to the formation types (I, C+, C–) were found within the experimental uncertainties. Then, a linear function of $2W(F+B) = (-0.067 \pm 0.011)\ A + (14.7 \pm 1.1)$, as the first approximation, was obtained by the

TABLE 1: Relevant Nuclear Data

Nuclide	Half life	Eγ(keV)	b.r.(%)	TYPE*3	Detec.*4	Nuclide	Half life	Eγ(keV)	b.r.(%)	TYPE	Detec.	Nuclide	Half life	Eγ(keV)	b.r.(%)	TYPE	Detec.
Ba-131	11.50d	496.3	46.8	C+	T, C	Tc-96	4.28d	849.9	97.6	I	C	Rb-81	4.576h	190.3	64.0	C+	T
Ba-129m	2.17h	182.3*1	47*1	C+	T, C	Nb-96	23.35h	1091.3*2	48.5*2	I	T, C	Br-77	2.377d	520.7	22.4	C+	C
Ba-129	2.23h	214.3*1	9.9*1	C+	T	Nb-95	34.98d	765.8	99.8	I	T, C	As-76	1.097d	559.1	45	I	T
Ba-128	2.43d	273.4	14.5	C+	T, C	Zr-95	64.02d	756.7	54.5	C-	T, C	Se-75	119.8d	264.7	58.5	C+	T, C
Ba-126	1.67h	233.6	20	C+	T	Nb-92m	10.15d	934.5	99.1	I	C	As-74	17.77d	595.8	59.4	I	T, C
Ag-113	5.37h	298.6	10	C-	T	Sr-92	2.71h	1383.9	90	C-	T, C	Ga-73	4.86h	297.3	79.8	C-	T
Ag-112	3.130h	617.4	43	I	T	Sr-91	9.63h	749.8	23.6	C-	T, C	As-72	1.08d	834.0	79.5	I	T
Ag-110m	249.8d	657.8	94.0	I	T, C	Y-90m	3.19h	202.5	97.3	I	T, C	Ga-72	14.10h	834.0	95.6	I	T, C
Ag-106m	8.28d	717.3	28.9	I	T	Zr-89	3.267d	909.1	99.9	C+	T, C	Zn-72	1.94d	144.7	82.9	C-	T, C
Ag-105	41.29d	344.5	41.4	C+	T	Zr-88	83.4d	392.9*2	97.3*2	C+	T, C	As-71	2.720d	175.0	82	C+	T
Rh-105	1.473d	318.9	19.2	C-	C	Y-88	106.7d	898.0	93.7	I	T, C	Zn-71m	3.96h	386.3	93	C-	T, C
Ru-105	4.44h	724.3	47.3	C-	C	Y-87m	13.37h	380.8	78.1	C+	T	Zn-69m	13.76h	438.6	94.8	I	T
Ag-104	1.15h	767.6	66	I	T	Y-87	3.33d	484.8	89.7	C+	T, C	Ni-66	2.28d	D1039.2	7.4	C-	T
Ag-103	1.10h	118.7	31	C+	T	Sr-87m	2.803h	388.5	82.1	I	T	Ni-65	2.517h	1481.8	23.6	C-	T, C
Ru-103	39.26d	497.1	90.9	C-	T, C	Rb-86	18.63d	1077.0	8.64	I	T, C	Fe-59	44.50d	1099.3	56.5	C-	T, C
Mo-99	2.748d	D140.5	90.7	C-	T, C	Rb-84	32.77d	881.6	69.0	I	T, C	Mn-56	2.579h	846.8	98.9	C-	C
Nb-98b	51.3min	787.4	93.4	I	T	Sr-83	1.350d	762.7	30	C+	T	Sc-46	83.79d	889.3	100	I	C
Ru-97	2.9d	215.7	85.6	C+	C	Rb-83	86.2d	520.4	44.7	C+	T, C	K-43	22.3h	617.5	79.2	C-	T
Nb-97	1.20h	657.9	98.4	I	T	Rb-82m	6.472h	776.5	84.4	I	T	K-42	12.36h	1524.7	18.1	I	T
Zr-97	16.91h	743.4	93.1	C-	T, C	Br-82	1.471d	698.4	28.5	I	C						

Nuclear data are from Ref. 31 except for *1 from Ref. 33 and *2 from Ref. 32.

*3: I: independent yield; C-: cumulative yield by β^- decay; C+: cumulative yield by β^+ decay and/or electron capture.

*4: Identification in Au target (T) or Mylar catcher (C).

D: γ-ray of the daughter in equilibrium.

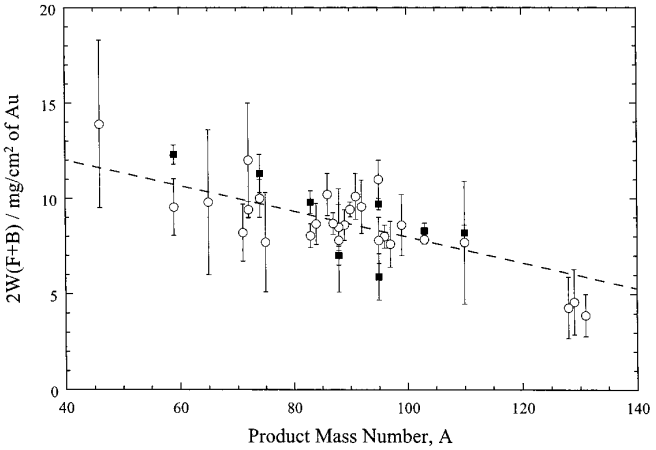

Figure 1. Measured mean ranges $2W(F+B)$ in unit of mg/cm² of Au as a function of product mass number A. The present results are shown by open circles, and those by Areskoug et al.[23] at E_0 = 600 MeV are shown by closed squares.

least squares fitting as shown by a dashed line in the figure. The quality of this fitting is fairly good because all of the $2W(F+B)$ values can be well reproduced within 2 σ of the experimental errors. By using this relation the reaction yields of the nuclides observed only in the target were obtained after correcting their recoil losses, and the relative yields of the nuclides found only in the catcher foils were normalized to the absolute ones. Thus the absolute yields of the 58 products in the mass range of A = 42–131 were obtained, and they are given in unit of μb per equivalent quanta (μb/eq.q.) in Table A1 in Appendix. The yield values in italics were obtained from the radioactivities assayed in the catcher foil. In general the yield values increase steeply with an increase of E_0 up to 600 MeV and increase gradually at higher E_0, indicating the resonance-type excitation function mainly attributed to the (3,3) resonance. It is noted that the saturation of the reaction yield above 600 MeV is reasonably consistent with the E_0-independent recoil properties such as forward-to-backward yield ratios and the kinetic energies of the residual nuclei.[24]

3.2. Charge Distribution. In the present work, the charge distribution $Y_{CD}(Z)$ among the isobars of a certain product mass number A, was assumed to be represented by the following Gaussian function:

$$Y_{CD}(Z) = Y_{CD}(Z_p)\cdot\exp\left\{\frac{-(Z-Z_p)^2}{C_Z}\right\}, \quad (1)$$

where, $Y_{CD}(Z_p)$ is the maximum yield of the charge distribution, Z_p being the most probable charge. The width parameter C_Z was assumed to be constant, irrespectively of A, and Z_p to be a linear function of A, i.e., $Z_p = RA + S$. By assuming the Unchanged Charge Distribution (UCD), the parameter R is related to a charge-to-mass ratio of a fissioning nucleus as R = 79 / (197−ν_{pre}), ν_{pre} being the number of prefission neutrons. The parameter S is a measure of the number of average post fission neutrons ν_{post} as $S = 79\nu_{post}$ / (197−ν_{pre}). The eq 1 was fitted to the experimental yields by a least squares method. For cumulative yields, a sum of the yields of a suitable number of isobars was fitted. The yields of the product nuclei in a metastable state were excluded from the present analysis. The results of yield measurements of ^{46,47,48}Sc and ^{56,57,58,60}Co from ^{197}Au target in the previous study[6] were also included in the present analysis. The four free parameters $Y_{CD}(Z_p)$, C_Z, R, and S were determined at representative eleven energies of E_0 = 1100, 1000, 900, 800, 700, 600, 500, 450, 400, 350, and 300 MeV. As an example, the charge distributions obtained at E_0 = 1100 MeV are shown in Figure 2 by solid curves for the representative mass chains of A = 56, 72, 83, 88, 95, 97, 103, and 105, in which more than two yield data were obtained. The independent yields (I), the cumulative yields by β⁻ decay (C–) and by β⁺ decay and/or electron capture (C+) are shown by open circles, closed triangles, and closed squares, respectively.

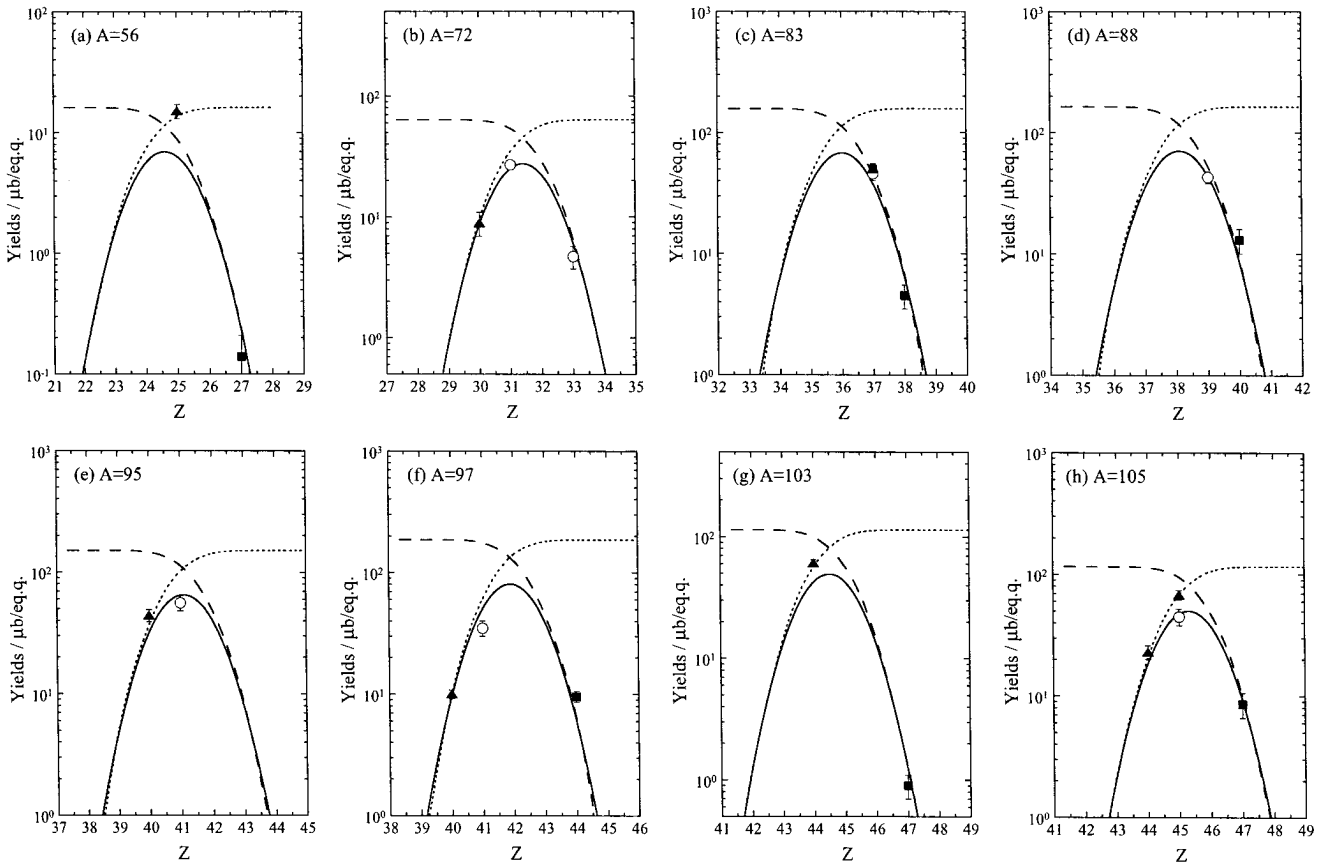

Figure 2. Charge distributions for the mass chains of (a) 56, (b) 72, (c) 83, (d) 88, (e) 95, (f) 97, (g) 103, and (h) 105 at E_0 = 1100 MeV. The independent yields (I), the cumulative yields by β⁻ decay (C–), and by β⁺ decay and/or electron capture (C+) are shown by open circles connected by a solid curve, closed triangles connected by a dotted curve, and closed squares connected by a dashed curve, respectively.

The cumulative yields calculated are shown by a dotted curve for C– and by a dashed curve for C+ by integrating the independent $Y_{CD}(Z_p)$ curve. It seems that the results of these fittings are fairly good and the present assumptions in eq 1 are reasonable.

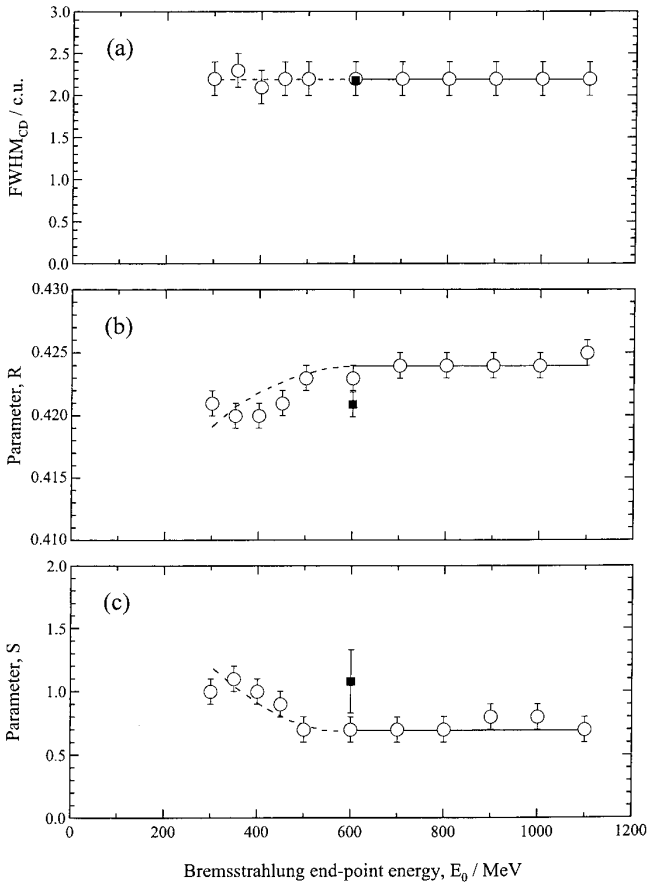

Figure 3. Charge distribution parameters (a) $FWHM_{CD}$, (b) R, and (c) S as a function of E_0. The present results are shown by open circles, and those by Areskoug et al.[23] at E_0 = 600 MeV are shown by closed squares.

The full width at half maximum of the charge distribution ($FWHM_{CD}$) in charge unit (c.u.) instead of C_Z and the parameters R and S are shown as a function of E_0 by open circles in Figures 3a–3c, respectively, together with those reported by Areskoug et al.[23] at E_0 = 600 MeV by closed squares. The $FWHM_{CD}$ (Figure 3a) shows E_0-independence at the studied E_0 within the quoted errors, and the weighted mean value of 2.2 ± 0.1 c.u. agrees well with that reported by Areskoug et al.[23] at E_0 = 600 MeV. On the other hand, the parameter R (Figure 3b) increases slightly with an increase of E_0 and becomes a constant value of R = 0.424 ± 0.001 above 600 MeV, which implies eleven-neutron emission before fission (ν_{pre} = 11) as deduced from the UCD assumption. The parameter S (Figure 3c) is also independent of E_0 above 600 MeV and the weighted mean value of 0.7 ± 0.1 implies the average two post neutrons (ν_{post} = 2). The variations of the R and S values below 600 MeV may reflect a change in the excitation energy, though the number of the measured isobars is small and the yield data are accompanied with large errors at lower energies. The R and S values reported by Areskoug et al.[23] at E_0 = 600 MeV are consistent with the present results within 2 σ of the experimental uncertainties.

3.3. Mass Yield Distribution. By using the charge distribution parameters $Y_{CD}(Z_p)$, C_Z, R, and S determined above, the total chain yields in unit of μb/eq.q. were evaluated for the mass chains of A = 42, 43, 46–48, 56–60, 65, 66, 71–77, 82–84, 86–89, 91, 92, 95–97, 99, 103, 105, 112, 126, 128, 129, and 131. The total chain yields calculated at E_0 = 1100, 900, 700, 500, and 300 MeV are shown in Figure 4 as a function of the product mass number (A) by open circles, closed triangles, open squares, closed inverse triangles, and open diamonds, respectively. The mass yield distributions seem to be symmetric with a maximum around A = 90. In the present work the mass yield distribution, $Y_{MD}(A)$, is assumed to be represented by the following Gaussian function,

$$Y_{MD}(A) = Y_{MD}(A_p)\cdot\exp\left\{\frac{-(A-A_p)^2}{C_A}\right\}, \quad (2)$$

where, $Y_{MD}(A_p)$ is the maximum of the mass distribution, A_p being the most probable mass, and C_A is the width parameter.

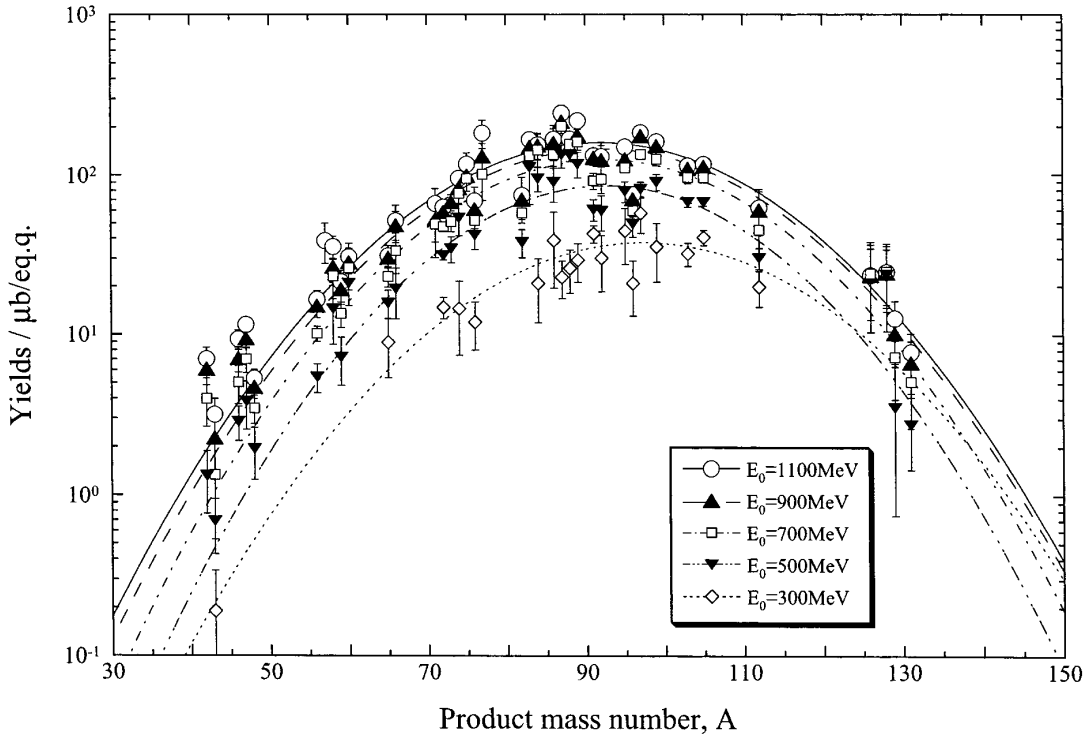

Figure 4. Mass yield curves of the photofission of ^{197}Au at E_0 = 1100, 900, 700, 500, and 300 MeV. See text for the details.

The total chain yields, except for the data at A = 42, 47, 82, and 96, which were largely deviated from the expected Gaussian curve, were fitted by eq 2 as shown by the different curves for each energy in Figure 4. The shape of the mass yield curves are almost the same above 500 MeV, though the absolute yields increase slightly with an increase of E_0. The mass yields at E_0 = 300 MeV, however, are quite smaller and the A_p value is somewhat higher than those at higher energies.

The relative mass yield curves reported by Komar et al.[22] at E_0 = 1000 MeV and Areskoug et al.[23] at E_0 = 600 MeV are applied to a comparison. In order to investigate the consistency of the mass yield curves obtained by the different methods and at the different energies, the A_p value and the full width at half maximum ($FWHM_{MD}$) are shown as a function of E_0 in Figures 5a and 5b, respectively. The A_p value decreases with an increase of E_0 from 97 ± 2 m.u. at E_0 = 300 MeV to a constant value of 92 ± 1 m.u. at $E_0 \geq$ 600 MeV. This constant value at $E_0 \geq$ 600 MeV is reasonable because the mass number of the fissioning nucleus was estimated to be A_f = 186 m.u. (ν_{pre} = 11) from the charge distribution parameter R based on the UCD assumption. The A_p value reported by Areskoug et al.[23] at E_0 = 600 MeV agrees well with the present result, but that by Komar et al.[22] at E_0 = 1000 MeV is higher by 5 m.u. because they assumed the mass number of the fissioning nucleus to be A_f = 194 m.u. On the other hand, the $FWHM_{MD}$ values are independent of E_0 at the studied energies within the experimental uncertainties, though a slightly increasing trend appears at E_0 < 600 MeV. The weighted mean value of 39 ± 1 m.u. at $E_0 \geq$ 600 MeV is equal to that measured by Komar et al.[22] by the coincident energy measurements of fragment pairs. However the $FWHM_{MD}$ value reported by Areskoug et al.[23] at E_0 = 600 MeV is lower by about 8 m.u. ($FWHM_{MD}$ = 30.9 ± 1.7 m.u.). As mentioned above, the charge distribution parameters $FWHM_{CD}$, R, and S reported by Areskoug et al.[23] at E_0 = 600 MeV are consistent with those obtained in the present work (See sect. 3. 2.). The discrepancy of $FWHM_{MD}$ may be attributed to the smaller mass range analyzed by Areskoug et al.[23] ($72 \leq A \leq 111$). Also noted is that Areskoug et al.[23] measured the cumulative yield of ^{59}Fe, but eliminated it from the analysis because the value of ^{59}Fe is anomalously higher than that deduced from their mass yield curve obtained at A = 72–111.

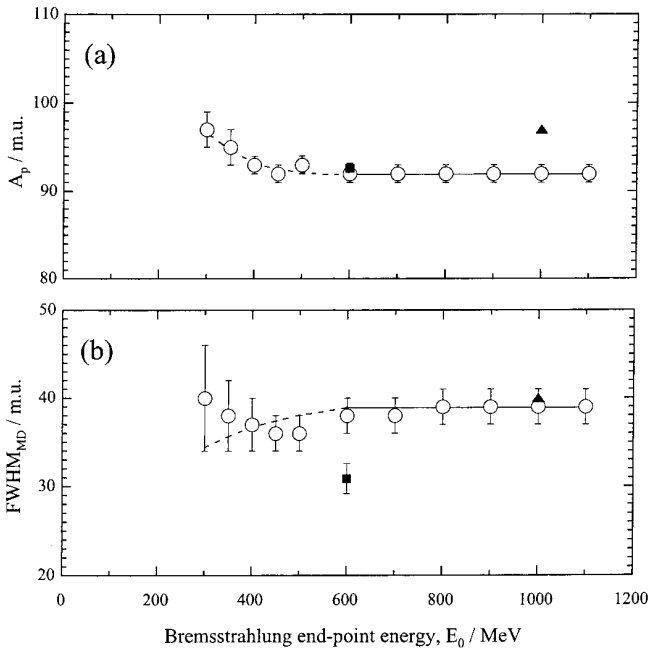

Figure 5. Variations of (a) the most probable mass A_p and (b) the full width at half maximum of the mass distribution $FWHM_{MD}$ as a function of E_0. The present results are shown by open circles, and those by Komar et al.[22] at E_0 = 1000 MeV and by Areskoug et al.[23] at E_0 = 600 MeV are shown by closed triangles and closed squares, respectively.

In the present work the product mass range measured was expanded widely to A = 42–131, and almost all of the total chain yields fell on the Gaussian curve. The anomaly of the ^{59}Fe yield suggested by Areskoug et al.[23] was not observed in the present work.

The total fission yields in unit of mb/eq.q. determined above from the mass yield curves are shown as a function of E_0 by open circles in Figure 6. As mentioned in Introduction, the total fission yields on ^{197}Au in unit of mb/eq.q. have been extensively measured with ionization chambers[7] and solid-state track detectors.[8,10–16] These results are compared in Figure 6 by the different symbols as shown in the inset of the figure. The results by the different authors are consistent with each other in the range of a factor of 2 except for the result by Kiely et al.[16] at E_0 = 580 MeV (an open diamond). The total fission yields increase steeply by about three orders of magnitude with an increase of E_0 from 100 MeV to 600 MeV and increase slightly at energies higher than E_0 = 600 MeV, indicating both the quasi-deuteron mechanism and the (3,3) resonance are main photoabsorption channels to induce fission process. In recent years the total fission cross sections have been intensively measured by quasi-monochromatic photon beams of energies up to 300 MeV,[17–21] and the detailed structure of the excitation function of the photofission of ^{197}Au has become clear. Unfortunately these beams are too low in intensities at present for our radiochemical studies.

The many radiochemical cross section measurements were performed for the proton-induced fission of ^{197}Au at the various proton energies.[34–44] Since almost all of the proton data were obtained by a nondestructive γ-ray measurement of the irradiated Au target, the number of nuclides measured are quite small and insufficient for the same analysis as applied in the present work. Therefore, the ratios of the reported cross sections of the proton reaction at E_p = 1000, 800, 600, 400, 300, and 200 MeV to the yields of the photon reaction at E_0 = 1000 MeV were calculated for some representative products of ^{46}Sc (I), ^{58}Co (I), ^{59}Fe (C–), ^{60}Co (I), ^{74}As (I), ^{75}Se (C+), ^{82}Br (I), ^{83,84,86}Rb (C+, I, I), ^{87,88}Y (C+, I), ^{89,95}Zr (C+, C–), ^{96}Tc (I), ^{103}Ru (C–), ^{105}Ag (C+), and ^{131}Ba (C+), based on our compilation of the cross section data in References 34–44. They are shown as a function of the product mass number A in Figure 7, all normalized to 1 at A = 103 (^{103}Ru), because the cross sections of the neutron rich isotope of ^{103}Ru are independent of E_p in the range of E_p = 200–1000 MeV.[38,39,41,42,44] The ratios at E_p = 300 and 400 MeV are almost unity (a dashed line), indicating the same mass yield shape as the photofission at E_0 = 1000 MeV. This may be reasonably understood, because the effective photons to induce fission process are mainly in the (3,3) resonance with a peak energy around 300 MeV. This fact

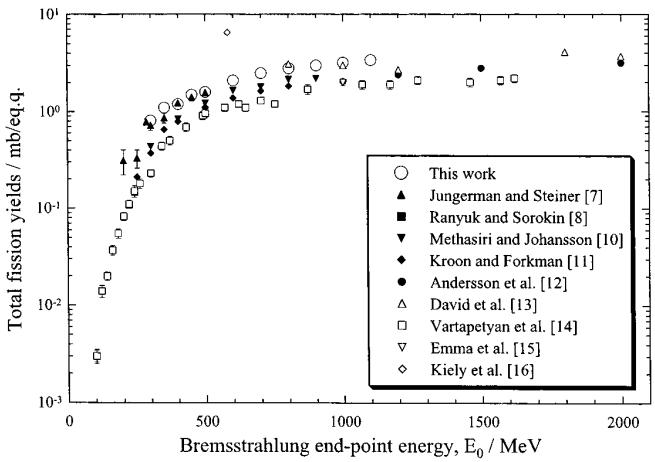

Figure 6. Total photofission yields of ^{197}Au in unit of mb per equivalent quanta (mb/eq.q.) as a function of E_0. See text for the details.

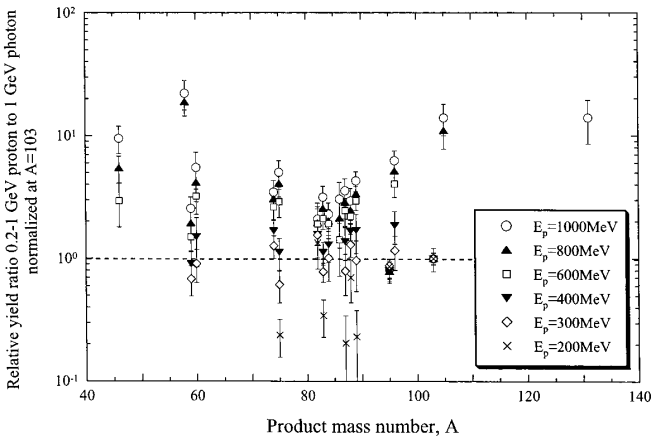

Figure 7. Ratios of the cross sections of the proton reactions at E_p = 1000, 800, 600, 400, 300, and 200 MeV to the yields of the photon reaction at E_0 = 1000 MeV as a function of product mass number A, normalized to 1 at A = 103 (^{103}Ru). See text for the details.

may imply that the difference in the initial interactions of photons and protons with nuclei does not affect the fissioning process. A few physical investigations of the mass yield curve, which is based on the coincident energy measurements of the fragment pairs, are also available at E_p = 1000 MeV.[45,46] The $FWHM_{MD}$ values of 54.5 ± 0.6 m.u. reported by Kotov et al.[45] and 46.9 m.u. by Andronenko et al.[46] are discrepant with each other and both are higher than the present photon result of 39 ± 1 m.u. at $E_0 \geq 600$ MeV. The intensive cross section measurements in the proton-induced fission of ^{197}Au are strongly desired in order to determine charge and mass yield distributions and to compare them further with the present photofission results.

The contributions of the spallation process in the observed yields were estimated by the CDMD formula[4] using the parameter set reported in Reference 2. The spallation yields were estimated to be one order of magnitude higher than the observed yields for the barium isotopes, for which the spallation contributions are deduced to be the largest. The parameter set in Reference 2 was determined based on the yield data of the near-target isotopes produced in the (γ, 0–5pxn) reactions, and might not be appreciable to such far-target isotopes as those in the barium region. An extensive yield measurements of rare earth elements are under study in order to clarify the difference in the charge and mass yield distributions between fission and spallation in the region of barium and light rare-earth isotopes. Recently, the yields of light nuclei such as ^{7,10}Be, ^{22,24}Na and ^{28}Mg from ^{197}Au were measured.[6] It was found that they are more than one order of magnitude higher than those extrapolated from the mass yield curve of fission, indicating different reaction mechanism; fragmentation. All of the mass yield data in Figure 4 are well reproduced by the Gaussian curves, indicating that the contributions of other reaction processes such as spallation and fragmentation are negligible within the experimental uncertainties.

It is interesting to compare the charge and mass yield distributions obtained in the present study with those calculated by a Monte-Carlo intranuclear cascade-evaporation code for photonuclear reactions. Previously, the cross sections and/or reaction yields of the photopion and photospallation reactions and the kinetic energies of the photospallation products were systematically compared with the Photon-Induced Intranuclear Cascade Analysis (PICA) code,[47,48] and various important information related to the nuclear structure and reaction mechanism was pointed out;[5,25,26,49–53] especially a requirement of nuclear medium effect in heavy nuclei with $A_t \geq 100$ in the PICA model was emphasized. Very recently, several modifications have been performed for the original PICA code and the fission process will be included in the calculation by Sato.[54] A comparison with the advanced PICA calculation[54] will be reported elsewhere, together with the same yield measurements of the photofission of ^{209}Bi, which are under study in our group.[55]

It was found that the charge distribution parameters (C_Z, R, and S) and the mass yield distribution parameters (A_p and C_A) as well as the recoil properties discussed in the separate paper[24] are all independent of E_0 above 600 MeV. It is concluded that the photofission process of ^{197}Au attains to the limiting behavior above 600 MeV as found in our previous studies of photospallation[1–3] and simple photopion reactions.[5,25,26] The measurements at E_0 < 300 MeV are strongly desired, because the different contributions of the giant dipole resonance, the quasi-deuteron mechanism, and the (3,3) resonance are included, and the change in the fission characters with E_0 is expected. A measurement at E_0 = 65 MeV, where only the giant dipole resonance and the quasi-deuteron mechanism contribute, was performed by using the 300 MeV electron linac of the Laboratory of Nuclear Science (LNS) of Tohoku University. The preliminary result of the symmetric mass yield distribution with A_p = 99 ± 1 and $FWHM_{MD}$ = 20 ± 1 m.u., which is quite different from the present results at $E_0 \geq$ 300 MeV, was obtained. The results will be reported elsewhere.

Acknowledgment. The authors would like to express their gratitude to Drs. H. Okuno and K. Masumoto, and the ES crew members of the High Energy Accelerator Research Organization at Tanashi, for their invaluable cooperations in the course of experiments. This work was supported in part by the Grant-in-Aid for Scientific Research (07304077) of the Ministry of Education, Science and Culture of Japan.

Appendix

TABLE A1: Yields of 58 Fission Products from ^{197}Au in Unit of μb per Equivalent Quanta (μb/eq.q.)

E_0 (MeV)	^{131}Ba (C+)	^{131}Ba (C+)	^{129m}Ba (C+)	^{129m}Ba (C+)	^{129}Ba (C+)	^{128}Ba (C+)	^{128}Ba (C+)	^{126}Ba (C+)	^{113}Ag (C-)
1100	6.79 ± 0.73		1.57 ± 0.11		4.70 ± 0.52	5.37 ± 0.49		0.981 ± 0.164	7.20 ± 0.76
1000	6.5 ± 0.4	*4.4 ± 1.1*	2.1 ± 0.5	*1.5 ± 0.5*	3.9 ± 2.3	9.7 ± 1.6	*6.4 ± 2.1*	2.7 ± 0.8	
950									
900									9.48 ± 0.53
800									8.59 ± 0.61
700			1.01 ± 0.18		2.31 ± 0.84	7.73 ± 1.71		1.36 ± 0.65	7.19 ± 0.36
650									
550									
500									5.82 ± 0.45
450	1.62 ± 0.63		0.413 ± 0.090		0.591 ± 0.387	4.96 ± 1.04			
400									6.37 ± 0.34
350									
300									3.82 ± 0.86

I: independent yield; C-: cumulative yield by β^- decay; C+: cumulative yield by β^+ decay and/or electron capture.
Yield values in italics were obtained from the activities in the catcher foils.

TABLE A1: (Continued)

E_0 (MeV)	^{112}Ag (I)	^{110m}Ag (I)	^{110m}Ag (I)	^{106m}Ag (I)	^{105}Ag (C+)	^{105}Rh (C-)	^{105}Ru (C-)	^{104}Ag (I)	^{103}Ag (C+)
1100	7.91 ± 0.80	9.62 ± 0.89	*9.2 ± 1.2*	3.41 ± 0.51	6.90 ± 0.79	60 ± 5	22 ± 2	1.85 ± 0.20	0.905 ± 0.125
1000			*13 ± 5*	3.24 ± 0.59		65 ± 4	19 ± 2		0.769 ± 0.192
950						66 ± 8	19 ± 2		
900	11.8 ± 0.5	11.1 ± 1.2	*7.9 ± 3.6*	6.04 ± 0.67	8.66 ± 0.99	73 ± 5	24 ± 2	2.03 ± 0.13	0.815 ± 0.089
800	12.0 ± 0.5	10.1 ± 1.3	*11 ± 4*	5.72 ± 0.91	8.23 ± 1.25	64 ± 4	21 ± 2	1.90 ± 0.12	0.871 ± 0.071
700	8.73 ± 0.29	7.88 ± 0.83	*13 ± 4*	3.01 ± 0.42	7.04 ± 0.66	68 ± 4	23 ± 2	1.34 ± 0.10	0.511 ± 0.082
650		10.3 ± 2.1		4.07 ± 0.68	10.0 ± 2.9	58 ± 5	19 ± 1		
550		11.1 ± 2.1		5.86 ± 1.25	5.08 ± 1.32	66 ± 9	18 ± 2	0.891 ± 0.138	
500	7.33 ± 0.32	8.80 ± 0.92		2.37 ± 0.32	4.58 ± 0.31	43 ± 6	16 ± 1	0.778 ± 0.087	0.189 ± 0.127
450	4.23 ± 0.28	5.07 ± 0.84		1.54 ± 0.69	3.46 ± 0.46				
400	6.43 ± 0.26	6.38 ± 0.85		1.56 ± 0.39		32 ± 4	12 ± 1	0.580 ± 0.070	0.295 ± 0.134
350						36 ± 5	11 ± 1		
300	5.55 ± 0.93	9.71 ± 6.71				35 ± 9	8.0 ± 1.2	0.279 ± 0.144	

TABLE A1: (Continued)

E_0 (MeV)	^{103}Ru (C-)	^{103}Ru (C-)	^{99}Mo (C-)	^{99}Mo (C-)	^{98b}Nb (I)	^{97}Ru (C+)	^{97}Nb (I)	^{97}Zr (C-)	^{97}Zr (C-)
1100	61.3 ± 2.3	*62 ± 3*	50.4 ± 2.3	*60 ± 2*	11 ± 2	*9.6 ± 0.6*	29 ± 2	9.06 ± 0.62	*9.1 ± 0.6*
1000	64.5 ± 2.8	*64 ± 3*		*54 ± 2*	11.5 ± 1.0	*9.8 ± 0.7*	33.4 ± 1.5	8.5 ± 0.7	*10 ± 1*
950	58.6 ± 2.6	*59 ± 3*	57 ± 2	*62 ± 3*		*8.9 ± 2.1*		9.6 ± 0.7	*10 ± 2*
900	65.8 ± 2.5	*65 ± 3*		*61 ± 2*		*8.8 ± 0.6*		9.0 ± 1.1	*9.6 ± 0.6*
800	60.2 ± 3.0	*57 ± 2*	48 ± 3	*61 ± 3*		*9.6 ± 0.7*		11.1 ± 0.7	*9.5 ± 0.5*
700	60.0 ± 2.5	*57 ± 3*		*51 ± 3*	9.0 ± 0.7	*8.0 ± 0.6*	30 ± 2		*8.5 ± 0.5*
650	53.3 ± 2.6	*54 ± 3*		*53 ± 3*				10.6 ± 0.7	*8.7 ± 0.5*
550	48.7 ± 7.5	*54 ± 4*		*49 ± 3*	9.6 ± 1.0		26 ± 2		*7.9 ± 1.3*
500	42.4 ± 2.6	*39 ± 2*	40.0 ± 2.6	*39 ± 2*	14 ± 3		22 ± 3	6.45 ± 0.53	*6.7 ± 0.7*
450									
400	31.8 ± 1.7	*32 ± 2*	26.0 ± 1.8	*32 ± 2*			30 ± 20	4.87 ± 0.34	*5.3 ± 0.6*
350	26.3 ± 2.0	*24 ± 2*	39 ± 8	*29 ± 2*				5.3 ± 0.5	*4.9 ± 0.9*
300	17.8 ± 2.2	*18 ± 7*	12 ± 2	*22 ± 2*				5.07 ± 0.97	*4.6 ± 1.0*

TABLE A1: (Continued)

E_0 (MeV)	^{96}Tc (I)	^{96}Nb (I)	^{96}Nb (I)	^{95}Nb (I)	^{95}Nb (I)	^{95}Zr (C-)	^{95}Zr (C-)	^{92m}Nb (I)	^{92m}Nb (I)
1100	*8.7 ± 0.9*	29 ± 2	*28 ± 2*	40 ± 4	*52 ± 3*	47.0 ± 2.3	*40 ± 2*		*2.3 ± 0.6*
1000	*9.9 ± 1.1*	30.1 ± 1.3	*28 ± 2*	48.1 ± 2.0	*60 ± 4*	36 ± 4	*42 ± 3*	3.90 ± 0.41	*4.4 ± 0.6*
950	*7.7 ± 1.3*		*25 ± 4*		*50 ± 6*	40 ± 7	*38 ± 7*		*6.0 ± 1.1*
900	*8.8 ± 0.7*		*26 ± 2*		*54 ± 3*	43 ± 3	*46 ± 3*		*3.9 ± 0.6*
800	*9.1 ± 0.9*		*24 ± 2*		*51 ± 3*	42.3 ± 2.8	*38 ± 3*		*3.4 ± 0.8*
700	*5.6 ± 0.8*	20 ± 1	*24 ± 2*	40 ± 3	*44 ± 3*		*37 ± 3*	4.5 ± 2.1	*2.4 ± 0.7*
650	*5.3 ± 1.2*		*21 ± 2*		*41 ± 3*	29.9 ± 2.7	*33 ± 4*		*3.4 ± 1.1*
550	*13 ± 4*	22 ± 2	*24 ± 4*	40 ± 3	*50 ± 7*		*36 ± 5*	4.6 ± 1.8	
500	*5.4 ± 1.2*	22 ± 3	*17 ± 2*	25 ± 14	*38 ± 3*	29.2 ± 1.7	*26 ± 4*		*2.5 ± 1.1*
450									
400	*2.5 ± 1.2*	20 ± 10	*14 ± 2*		*24 ± 3*	20.0 ± 1.6	*22 ± 4*		
350			*7.5 ± 1.2*		*25 ± 3*	16 ± 6	*22 ± 5*		
300			*7.7 ± 1.7*			13.2 ± 6.4			

TABLE A1: (Continued)

E_0 (MeV)	^{92}Sr (C-)	^{92}Sr (C-)	^{91}Sr (C-)	^{91}Sr (C-)	^{90m}Y (I)	^{90m}Y (I)	^{89}Zr (C+)	^{89}Zr (C+)	^{88}Zr (C+)
1100	7.9 ± 0.6	*8.4 ± 0.5*	16.3 ± 1.2	*18 ± 3*	56.4 ± 3.0	*55 ± 2*	29.2 ± 1.9	*29 ± 2*	14.9 ± 1.0
1000		*9.7 ± 1.0*		*19 ± 2*	46.6 ± 1.2	*54 ± 3*	26 ± 3	*26 ± 2*	11 ± 2
950		*11 ± 2*		*26 ± 4*	48.0 ± 2.0	*50 ± 2*	20 ± 3	*22 ± 3*	9.3 ± 2.0
900		*11 ± 1*		*24 ± 2*	48.7 ± 1.2	*56 ± 2*	26 ± 2	*25 ± 1*	15 ± 2
800	7.5 ± 0.4	*8.1 ± 0.6*	15.9 ± 1.0	*21 ± 2*	43.1 ± 1.6	*49 ± 2*	21.5 ± 1.5	*22 ± 2*	4.80 ± 1.33
700		*9.0 ± 0.6*		*18 ± 2*	41.6 ± 1.2	*46 ± 2*		*19 ± 1*	
650	6.2 ± 0.5	*8.7 ± 0.7*	15.2 ± 1.0	*16 ± 2*	39.3 ± 1.5	*43 ± 2*	17.2 ± 1.3	*15 ± 3*	
550		*9.6 ± 1.3*			32.5 ± 1.0	*36 ± 2*		*13 ± 2*	
500	5.0 ± 0.5	*7.0 ± 0.8*	10.2 ± 1.0	*13 ± 2*	33.5 ± 2.4	*31 ± 2*	11.3 ± 1.0	*11 ± 2*	4.99 ± 0.70
450									
400	3.8 ± 0.3	*5.1 ± 0.5*	9.72 ± 0.60	*12 ± 2*	27.0 ± 2.7	*23 ± 1*	4.72 ± 0.64	*7.3 ± 1.3*	1.94 ± 0.71
350	2.7 ± 0.6	*5.4 ± 0.8*	7.65 ± 0.93	*9.8 ± 2.5*	16.0 ± 0.6	*17 ± 1*	6.6 ± 1.1		6.7 ± 2.5
300	2.9 ± 0.2	*3.6 ± 0.8*	7.92 ± 1.46		10.0 ± 0.6	*13 ± 1*	4.49 ± 1.26		

TABLE A1: (Continued)

E_0 (MeV)	^{88}Zr (C+)	^{88}Y (I)	^{88}Y (I)	^{87m}Y (C+)	^{87}Y (C+)	^{87}Y (C+)	^{87m}Sr (C+)	^{86}Rb (I)	^{86}Rb (I)
1100	*13 ± 1*	48.8 ± 3.6	*39 ± 4*	43.0 ± 2.4	46.1 ± 2.6	*41 ± 2*	3.53 ± 0.30	56.7 ± 5.6	*68 ± 8*
1000	*13 ± 2*	46.8 ± 2.2		34.1 ± 0.9	39.0 ± 1.4	*38 ± 2*		55.6 ± 6.7	*58 ± 10*
950				33.4 ± 2.1	36.4 ± 3.0	*40 ± 3*		75.8 ± 23.4	*72 ± 28*
900	*13 ± 1*	42.9 ± 1.7	*44 ± 3*	32.9 ± 0.7	39.4 ± 1.2	*40 ± 2*		67.2 ± 7.5	*79 ± 8*
800	*7.2 ± 0.9*	36.2 ± 2.4	*37 ± 4*	27.1 ± 1.0	36.0 ± 3.0	*38 ± 2*	3.17 ± 0.23	48 ± 5	*73 ± 10*
700	*8.8 ± 1.0*	35.3 ± 1.5	*33 ± 3*	21.2 ± 0.7	30.2 ± 1.1	*31 ± 2*		66 ± 9	*66 ± 9*
650	*6.4 ± 2.1*	28.3 ± 2.3	*34 ± 5*	21.8 ± 1.0	26.6 ± 1.9	*26 ± 2*	3.15 ± 0.22	57 ± 8	
550		30.3 ± 2.2		15.0 ± 0.6	18.5 ± 0.9	*23 ± 2*		46.3 ± 12.7	*79 ± 22*
500		31.1 ± 3.1	*28 ± 3*	18.0 ± 1.4	19.1 ± 1.5	*16 ± 2*	1.40 ± 0.18	23.8 ± 6.2	*42 ± 11*
450									
400		19.6 ± 2.9	*19 ± 2*	10.9 ± 1.2	12.8 ± 1.4	*12 ± 1*	1.05 ± 0.14	28.4 ± 7.7	*32 ± 11*
350				5.41 ± 0.35	6.83 ± 0.59	*6.9 ± 1.3*			*62 ± 21*
300		3.11 ± 2.20		3.11 ± 0.38	3.93 ± 0.79		0.729 ± 0.273	36.6 ± 21.8	

TABLE A1: (Continued)

E_0 (MeV)	^{84}Rb (I)	^{84}Rb (I)	^{83}Sr (C+)	^{83}Rb (C+)	^{83}Rb (C+)	^{82m}Rb (I)	^{82}Br (I)	^{81}Rb (C+)	^{77}Br (C+)
1100	56.0 ± 3.2	*56 ± 3*	3.63 ± 0.71	52.1 ± 2.5	*48 ± 2*	14.0 ± 1.0	*21 ± 3*	8.91 ± 0.73	*16 ± 3*
1000	62.1 ± 4.5	*51 ± 3*		57.8 ± 3.9	*44 ± 3*	12.4 ± 1.1	*32 ± 3*	8.77 ± 1.03	*21 ± 4*
950	63.9 ± 5.2	*54 ± 4*			*47 ± 10*		*35 ± 5*		*24 ± 8*
900	63.2 ± 3.3	*57 ± 5*		54.3 ± 2.8	*51 ± 3*	13.3 ± 0.7	*23 ± 2*	9.38 ± 0.66	*13 ± 3*
800	43 ± 2	*50 ± 3*	3.99 ± 0.65	42.3 ± 4.2	*41 ± 4*	10.1 ± 0.6	*25 ± 2*	6.66 ± 0.68	*12 ± 3*
700	54 ± 4	*41 ± 3*		40.2 ± 3.3	*33 ± 3*	9.21 ± 0.65	*22 ± 2*	6.2 ± 0.7	*9.5 ± 2.1*
650	34 ± 2	*44 ± 3*	3.20 ± 0.95	36.1 ± 3.7	*29 ± 5*	5.27 ± 0.55	*22 ± 3*	4.06 ± 0.77	*13 ± 5*
550		*41 ± 3*			*42 ± 6*	5.39 ± 0.55		3.55 ± 0.87	
500	21.5 ± 4.9	*31 ± 3*			*34 ± 4*	4.01 ± 1.02	*15 ± 3*	2.22 ± 0.70	
450									
400	21.6 ± 3.7	*21 ± 3*			*12 ± 4*	3.55 ± 0.69	*5.8 ± 2.1*	1.78 ± 0.46	
350	15.4 ± 5.2	*18 ± 3*				1.45 ± 0.62	*12 ± 4*	0.626 ± 0.318	
300	7.32 ± 2.89					1.05 ± 0.28			

TABLE A1: (Continued)

E_0 (MeV)	^{76}As (I)	^{75}Se (C+)	^{75}Se (C+)	^{74}As (I)	^{74}As (I)	^{73}Ga (C-)	^{72}As (I)	^{72}Ga (I)	^{72}Ga (I)
1100	32 ± 2	18.3 ± 1.0	*14 ± 2*	24.4 ± 1.7	*26 ± 2*		5.4 ± 0.4		*27 ± 1*
1000	23 ± 1	18.6 ± 1.7	*14 ± 4*	19.6 ± 2.1	*30 ± 2*	23 ± 2	4.37 ± 0.26	23 ± 2	*27 ± 2*
950					*28 ± 3*	27.4 ± 1.1		27.0 ± 1.5	*26 ± 1*
900		16.3 ± 1.8	*13 ± 4*		*27 ± 2*				*25 ± 1*
800	25 ± 2	11.6 ± 1.3	*15 ± 4*	23 ± 1	*22 ± 2*		2.9 ± 0.5		*24 ± 1*
700	20 ± 1	11.9 ± 1.5	*14 ± 4*	13.5 ± 2.3	*21 ± 2*	18.2 ± 0.9	1.99 ± 0.16	18.0 ± 0.9	*21 ± 1*
650	22 ± 2	9.58 ± 1.74		18 ± 2	*22 ± 2*				*20 ± 1*
550	16 ± 1			13.1 ± 1.8	*22 ± 3*	18.5 ± 0.7	2.7 ± 0.4	17.4 ± 0.8	*16 ± 2*
500	14 ± 2			14 ± 2	*15 ± 2*		1.3 ± 0.4		*14 ± 1*
450									
400	11 ± 1			5.3 ± 0.8	*11 ± 2*				*9.9 ± 0.6*
350	11 ± 3					10.2 ± 0.8		7.07 ± 0.62	*7.9 ± 0.8*
300	4.7 ± 1.1			4.1 ± 1.4					*6.0 ± 0.8*

TABLE A1: (Continued)

E_0 (MeV)	^{72}Zn (C-)	^{72}Zn (C-)	^{71}As (C+)	^{71m}Zn (C-)	^{71m}Zn (C-)	^{69m}Zn (I)	^{66}Ni (C-)	^{65}Ni (C-)	^{65}Ni (C-)
1100		*8.6 ± 0.5*	2.9 ± 0.3	5.3 ± 0.3	*5.8 ± 0.4*		15 ± 3	18.9 ± 0.9	*17 ± 2*
1000		*8.9 ± 0.5*	1.56 ± 0.15		*6.8 ± 0.6*				*22 ± 3*
950		*10 ± 2*			*5.5 ± 1.0*		19 ± 4	15 ± 2	*24 ± 4*
900		*9.9 ± 0.4*			*6.2 ± 0.6*				*17 ± 2*
800	8.0 ± 0.6	*8.5 ± 0.5*	1.3 ± 0.3		*6.3 ± 0.5*	19 ± 1	16 ± 10	16.5 ± 1.4	*16 ± 2*
700	6.0 ± 0.5	*8.2 ± 0.4*	0.949 ± 0.136	6.6 ± 0.4	*4.9 ± 0.6*	14 ± 1	16 ± 4	11.8 ± 0.9	*14 ± 2*
650	8.6 ± 1.3	*7.0 ± 0.5*		7.3 ± 1.0	*4.9 ± 0.5*	15 ± 2			*13 ± 2*
550		*5.1 ± 0.8*	1.18 ± 0.22		*4.3 ± 0.7*				
500	3.47 ± 0.49	*4.0 ± 0.5*		3.3 ± 0.3	*3.6 ± 0.4*	8.79 ± 0.46	8.7 ± 4.1	10.2 ± 0.9	*11 ± 3*
450							8.7 ± 3.6	6.2 ± 0.8	
400	3.70 ± 0.24	*4.8 ± 0.6*		3.1 ± 0.3	*2.9 ± 0.3*	7.39 ± 0.35	5.5 ± 2.1	6.19 ± 0.82	*6.4 ± 1.5*
350	2.8 ± 1.0	*4.9 ± 1.0*		3.2 ± 0.5	*2.5 ± 0.5*	5.3 ± 0.7		7.6 ± 1.0	*8.5 ± 2.0*
300	3.30 ± 0.61	*4.5 ± 1.1*		2.8 ± 0.4	*2.6 ± 0.6*	2.96 ± 0.47		6.41 ± 1.33	*8.0 ± 0.3*

TABLE A1: (Continued)

E_0 (MeV)	^{59}Fe (C-)	^{59}Fe (C-)	^{56}Mn (C-)	^{43}K (C-)	^{42}K (I)
1100	17.7 ± 0.9	*15 ± 2*	*13 ± 1*	2.73 ± 0.15	2.3 ± 0.3
1000	16.7 ± 1.0	*17 ± 2*	*14 ± 1*		
950	18.2 ± 1.2	*20 ± 4*	*12 ± 1*	1.2 ± 0.3	1.9 ± 0.4
900	17.8 ± 1.1	*16 ± 2*	*13 ± 1*		
800	15.9 ± 1.1	*15 ± 2*	*11 ± 1*	1.9 ± 0.2	2.2 ± 0.2
700	12.4 ± 0.8	*12 ± 2*	*9.4 ± 0.5*		
650	10.9 ± 1.0	*7.2 ± 2.1*	*8.2 ± 0.5*	0.92 ± 0.29	
550			*6.4 ± 0.8*		
500	4.53 ± 1.34	*7.9 ± 2.2*	*3.8 ± 0.5*	0.53 ± 0.12	0.5 ± 0.2
450					
400	3.54 ± 0.69	*4.6 ± 2.2*	*3.3 ± 0.4*	0.4 ± 0.3	
350		*8.3 ± 4.0*	*2.7 ± 0.6*	0.22 ± 0.18	
300				0.26 ± 0.21	

References

(1) S. Shibata, M. Imamura, T. Miyachi, M. Mutou, K. Sakamoto, Y. Hamajima, M. Soto, Y. Kubota, M. Yoshida, and I. Fujiwara, Phys. Rev. C **35**, 254 (1987).

(2) S. R. Sarkar, M. Soto, Y. Kubota, M. Yoshida, T. Fukasawa, K. Matsumoto, K. Kawaguchi, K. Sakamoto, S. Shibata, M. Furukawa, and I. Fujiwara, Radiochim. Acta **55**, 113 (1991).

(3) S. R. Sarkar, Y. Kubota, T. Fukasawa, K. Kawaguchi, K. Sakamoto, S. Shibata, and I. Fujiwara, Radiochim. Acta **55**, 139 (1991).

(4) G. Z. Rudstam, Naturforsch. **21a**, 1027 (1966).

(5) K. Sakamoto, S. R. Sarkar, Y. Oura, H. Haba, H. Matsumura, Y. Miyamoto, S. Shibata, M. Furukawa, and I. Fujiwara, Phys. Rev. C **59**, 1497 (1999).

(6) H. Matsumura, K. Washiyama, H. Haba, Y. Miyamoto, Y. Oura, K. Sakamoto, S. Shibata, M. Furukawa, I. Fujiwara, H. Nagai, T. Kobayashi, and K. Kobayashi, Radiochim. Acta **88**, 313 (2000).

(7) J. A. Jungerman and H. M. Steiner, Phys. Rev. **106**, 585 (1957).

(8) Yu. N. Ranyuk and P. V. Sorokin, Sov. J. Nucl. Phys. **5**, 26 (1967).

(9) A. V. Mitrofanova, Yu. N. Ranyuk, and P. V. Sorokin, Sov. J. Nucl. Phys. **64**, 512 (1968).
(10) T. Methasiri and S. A. E. Johansson, Nucl. Phys. **A167**, 97 (1971).
(11) I. Kroon and B. Forkman, Nucl. Phys. **A179**, 141 (1972).
(12) G. Andersson, I. Blomqvist, B. Forkman, G. G. Jonsson, A. Järund, I. Kroon, K. Lindgren, B. Schrøder, and K. Tesch, Nucl. Phys. **A197**, 44 (1972).
(13) P. David, J. Debrus, U. Kim, G. Kumbartzki, H. Mommsen, W. Soyez, K. H. Speidel, and G. Stein, Nucl. Phys. **A197**, 163 (1972).
(14) G. A. Vartapetyan, N. A. Demekhina, V. I. Kasilov, Yu. N. Ranyuk, P. V. Sorokin, and A. G. Khudaverdyan, Sov. J. Nucl. Phys. **14**, 37 (1972).
(15) V. Emma, S. Lo Nigro, and C. Milone, Nucl. Phys. **A257**, 438 (1976).
(16) F. M. Kiely, B. D. Pate, F. Hanappe, and J. Peter, Z. Phys. A **279**, 331 (1976).
(17) V. Lucherini, C. Guaraldo, E. De Sanctis, P. Levi Sandri, E. Polli, A. R. Reolon, A. S. Iljinov, S. Lo Nigro, S. Aiello, V. Bellini, V. Emma, C. Milone, G. S. Pappalardo, and M. V. Mebel, Phys. Rev. C **39**, 911 (1989).
(18) J. B. Martins, E. L. Moreira, O. A. P. Tavares, J. L. Vieira, J. D. Pinheiro Filho, R. Bernabei, S. D'Angelo, M. P. De Pascale, C. Schaerf, and B. Girolami, Nuovo Cim. **101A**, 789 (1989).
(19) J. B. Martins, E. L. Moreira, O. A. P. Tavares, J. L. Vieira, L. Casano, A. D'Angelo, C. Schaerf, M. L. Terranova, D. Babusci, and B. Girolami, Phys. Rev. C **44**, 354 (1991).
(20) M. L. Terranova, O. A. P. Tavares, G. Ya Kezerashvili, V. A. Kiselev, A. M. Milov, N. Yu Muchnoi, A. I. Naumenkov, V. V. Petrov, I. Ya Protopopov, E. A. Simonov, E. de Paiva, and E. L. Moreira, J. Phys. G **22**, 511 (1996).
(21) M. L. Terranova, G. Ya Kezerashvili, A. M. Milov, S. I. Mishnev, N. Yu Muchnoi, A. I. Naumenkov, I. Ya Protopopov, E. A. Simonov, D. N. Shatilov, O. A. P. Tavares, E. de Paiva, and E. L. Moreira, J. Phys. G **24**, 205 (1998).
(22) A. P. Komar, B. A. Bochagov, A. A. Kotov, Yu. N. Ranyuk, G. G. Semenchuk, G. E. Solyakin, and P. V. Sorokin, Sov. J. Nucl. Phys. **10**, 30 (1970).
(23) M. Areskoug, B. Schrøder, K. Lindgren, G. Andersson, and B. Forkman, Nucl. Phys. **A226**, 93 (1974).
(24) H. Haba, M. Igarashi, K. Washiyama, H. Matsumura, M. Yamashita, K. Sakamoto, Y. Oura, S. Shibata, M. Furukawa, and I. Fujiwara, J. Nucl. Radiochem. Sci. (in press, 2000).
(25) K. Sakamoto, M. Yoshida, Y. Kubota, T. Fukasawa, A. Kunugise, Y. Hamajima, S. Shibata, and I. Fujiwara, Nucl. Phys. **A501**, 693 (1989).
(26) K. Sakamoto, Y. Hamajima, M. Soto, Y. Kubota, M. Yoshida, A. Kunugise, M. Masatani, S. Shibata, M. Imamura, M. Furukawa, and I. Fujiwara, Phys. Rev. C **42**, 1545 (1990).
(27) B. Johnsson, A. Järund, and B. Forkman, Z. Phys. A **273**, 97 (1975).
(28) K. Osada, T. Fukasawa, K. Kobayashi, Y. Hamajima, K. Sakamoto, S. Shibata, and I. Fujiwara, Res. Rept. Lab. Nucl. Sci. Tohoku Univ. **20**, 299 (1987).
(29) H. Haba, Ph. D. Thesis (Kanazawa Univ., 1999).
(30) Y. Hamajima (private communication, 1998).
(31) R. B. Firestone and V. S. Shirley, *Table of Isotopes, 8th ed.* (John Wiley and Sons, Inc., New York, 1996).
(32) E. Browne and R. B. Firestone, *Table of Radioactive Isotopes* (John Wiley and Sons, Inc., New York, 1986).
(33) U. Reus and W. Westmeier, At. Data Nucl. Data Tables **29**, 193 (1983).
(34) P. Kruger and N. Sugarman, Phys. Rev. **99**, 1459 (1955).
(35) G. Rudstam and G. Sørensen, J. Inorg. Nucl. Chem. **28**, 771 (1966).
(36) E. Hagebø and H. Ravn, J. Inorg. Nucl. Chem. **31**, 897 (1969).
(37) Y. W. Yu and N. T. Porile, Phys. Rev. C **12**, 938 (1975).
(38) S. B. Kaufman, M. W. Weisfield, E. P. Steinberg, B. D. Wilkins, and D. Henderson, Phys. Rev. C **14**, 1121 (1976).
(39) S. Krämer, B. Neidhart, and K. Bächmann, Inorg. Nucl. Chem. Letters **13**, 205 (1977).
(40) M. Lagarde-Simonoff and G. N. Simonoff, Phys. Rev. C **20**, 1498 (1979).
(41) S. B. Kaufman and E. P. Steinberg, Phys. Rev. C **22**, 167 (1980).
(42) Y. Asano, S. Mori, M. Noguchi, M. Sakano, K. Katoh, and K. Kondo, J. Phys. Soc. Japan **54**, 3734 (1985).
(43) Y. Asano, H. Kariya, S. Mori, M. Okano, and M. Sakano, J. Phys. Soc. Japan **57**, 2995 (1988).
(44) R. Michel, R. Bodemann, H. Busemann, R. Daunke, M. Gloris, H. -J. Lange, B. Klug, A. Krins, I. Leya, M. Lüpke, S. Neumann, H. Reinhardt, M. Schnatz-Büttgen, U. Herpers, Th. Schiekel, F. Sudbrock, B. Holmqvist, H. Condé, P. Malmborg, M. Suter, B. Dittrich-Hannen, P. -W. Kubik, H. -A. Synal, and D. Filges, Nucl. Instrum. Methods Phys. Res. B **129**, 153 (1997).
(45) A. A. Kotov, G. G. Semenchuk, L. N. Andronenko, M. N. Andronenko, B. L. Gorshkov, G. G. Kovshevnyi, V. R. Reznik, and G. E. Solyakin, Sov. J. Nucl. Phys. **20**, 251 (1975).
(46) L. N. Andronenko, A. A. Kotov, M. M. Nesterov, V. F. Petrov, N. A. Tarasov, L. A. Vaishnene, and W. Neubert, Z. Phys. A **318**, 97 (1984).
(47) T. A. Gabriel and R. G. Alsmiller Jr., Phys. Rev. **182**, 1035 (1969).
(48) T. A. Gabriel, M. P. Guthrie, and O. W. Hermann, Oak Ridge National Laboratory Report ORNL-4687 (1971).
(49) S. R. Sarkar, Y. Oura, K. Kawaguchi, A. Yazawa, K. Sakamoto, S. Shibata, and I. Fujiwara, Radiochim. Acta **62**, 7 (1993).
(50) Y. Oura, A. Yazawa, M. Yoshida, S. R. Sarkar, K. Sakamoto, S. Shibata, I. Fujiwara, and M. Furukawa, Radiochim. Acta **68**, 27 (1995).
(51) H. Haba, H. Matsumura, Y. Miyamoto, K. Sakamoto, Y. Oura, S. Shibata, M. Furukawa, and I. Fujiwara, J. Radioanal. Nucl. Chem. **239**, 133 (1999).
(52) H. Haba, H. Matsumura, K. Sakamoto, Y. Oura, S. Shibata, M. Furukawa, and I. Fujiwara, Radiochim. Acta **85**, 1 (1999).
(53) H. Haba, H. Matsumura, K. Sakamoto, Y. Oura, S. Shibata, M. Furukawa, and I. Fujiwara, Radiochim. Acta **88**, 375 (2000).
(54) T. Sato (private communication, 2000).
(55) H. Haba, M. Igarashi, M. Kasaoka, K. Washiyama, H. Matsumura, M. Yamashita, K. Sakamoto, Y. Oura, S. Shibata, M. Furukawa, and I. Fujiwara, Extended Abstracts of 5th International Conference on Nuclear and Radiochemistry (3-8 September 2000 in Switzerland Vol. 1, 24 (2000)).